



The Unified Gravel-Sand (*TUGS*) Model: Simulating Sediment Transport and Gravel/Sand Grain Size Distributions in Gravel-Bedded Rivers

Yantao Cui¹

Received 9 July 2006; revised 7 August 2007; accepted 14 August 2007; published 30 October 2007.

[1] This paper presents The Unified Gravel-Sand (*TUGS*) model that simulates the transport, erosion, and deposition of both gravel and sand. *TUGS* model employs the surface-based bed load equation of Wilcock and Crowe (2003) and links grain size distributions in the bed load, surface layer, and subsurface with the gravel transfer function of Hoey and Ferguson (1994) and Toro-Escobar et al. (1996), a hypothetical sand transfer function, and hypothetical functions for sand entrainment/infiltration from/into the subsurface. The model is capable of exploring the dynamics of grain size distributions, including the fractions of sand in sediment deposits and on the channel bed surface, and is potentially useful in exploring gravel-sand transitions and reservoir sedimentation processes. Simulation of three sets of large-scale flume experiments indicates that the model, with minor adjustment to the Wilcock-Crowe equation, excellently reproduced bed profile and grain size distributions of the sediment deposits, including the fractions of sand within the deposits. Simulation of a flushing flow experiment indicated that the sand entrainment function is potentially capable of simulating the short-term processes such as flushing flow events.

Citation: Cui, Y. (2007), The Unified Gravel-Sand (*TUGS*) Model: Simulating Sediment Transport and Gravel/Sand Grain Size Distributions in Gravel-Bedded Rivers, *Water Resour. Res.*, 43, W10436, doi:10.1029/2006WR005330.

1. Introduction

[2] Understanding the dynamics of grain size distributions, particularly the fractions of fine sediment (sand and finer) in channel bed deposits in salmonid bearing rivers is of grave importance. Adult salmonids select locations with favorable hydraulic conditions and appropriate grain size distributions to deposit their eggs, which generally incubate for a period of about two to five months [Beacham and Murray, 1990]. In addition to egg mortality due to exposures from redd scour during flood events, two other potential risks for incubating salmonid eggs are low survival rate due to low intragravel flow and entombment of fry, both of which are usually the result of high fine sediment content in the spawning habitats [e.g., Coble, 1961; Cooper, 1965; Phillips et al., 1975]. To date, only a few numerical sediment transport models attempted to predict the evolution of sand fraction in a gravel deposits. For example, Ferguson [2003] explored the emergence of abrupt gravel-sand transitions in rivers while Wu and Chou [2003] explored the effect of flushing flow with a numerical model; both models include gravel and sand. The models of Ferguson [2003] and Wu and Chou [2003] divided sediment into gravel and sand fractions while no detailed grain size distributions of either gravel or sand was simulated. In particular, the model of Wu and Chou [2003] applied a sediment transport equation that resembles the two-fraction

sediment transport equation of Wilcock [1998], while the model of Ferguson applied a sediment transport equation with similar concept as the two-fraction equation of Wilcock and Kenworthy [2002]. Few numerical models capable of simulating both gravel and sand are currently available because the interaction between sediment deposits and sediment particles in transport (bed load) is an extremely complex process, which is poorly understood, especially when both fine and coarse sediments are considered. It can be expected that the fraction of sand in a sediment deposit is positively correlated with sand supply, as implemented in Wu and Chou [2003]. However, other factors may significantly affect the deposition of sand in a sediment deposit of gravel-sand mixture, whether it is framework-supported or matrix-supported. Cui and Parker [1998], for example, suggested that the fractions of sand in sediment deposits of gravel-sand mixtures are highly correlated to the standard deviation of the gravel class of the sediment deposit: a sediment deposit composed only of coarse sediment with a smaller standard deviation means more uniform sediment particles, which implies more pore space available for fine sediment to infiltrate. It can be expected that a numerical model that describes the dynamics of gravel grain size distributions is potentially capable of addressing the concerns of Cui and Parker's [1998]. In addition, a model describing the grain size distributions of gravel will also allow for inclusion of particle abrasion, which can be critically important in modeling long-river reaches because particle abrasion accelerates the transport of sediment, as demonstrated by Cui and Parker [2005]. Most of the current fractional-based sediment transport models for gravel bed-

¹Stillwater Sciences, Berkeley, California, USA.

ded rivers treat fine sediment (sand and finer) as throughput load, thus excluding it from the simulation. An example of such a model is the gravel pulse model of *Cui and Parker* [2005], which applies the surface-based bed load equation of *Parker* [1990], an equation that excludes sand and finer particles. To include sand in the simulation of sediment transport, erosion, and deposition processes following removal of dams, *Cui and Wilcox* [2007] and *Cui et al.* [2006a, 2006b] assumed that gravel and sand transport by different processes (bed load versus suspended load) and at different timescales (years versus days). They further assumed that gravel and sand transport are weakly correlated and can be assumed to be independent of each other, thus allowing for application of their respective equations independently. The treatment of *Cui and Wilcox* [2007] and *Cui et al.* [2006a, 2006b] allowed for a simple evaluation of potential sand deposition over a gravel bed in the absence of a unified gravel-sand transport equation. The models of *Cui and Wilcox* [2007] and *Cui et al.* [2006a, 2006b], however, cannot be used for predicting subsurface sand fractions in the absence of a relation linking sand fractions in bed load, the surface layer and the subsurface.

[3] The recent *Wilcock and Crowe* [2003] sediment transport equation provides the first sediment transport relation that calculates both gravel and sand transport on a fractional-basis that accounts for the effect of surface sand fraction on particle mobility. A formulation is proposed herein as a first-order approximation, linking sand fractions in interface sediment (i.e., sediment to become part of subsurface during aggradation, and sediment to be eroded from subsurface during degradation) and the surface layer (more details about the surface, subsurface and interface are provided below in Section 2). In addition, hypothetical relations are proposed to calculate the entrainment of sand from the subsurface and infiltration of sand into the subsurface based on the concept for upward sand movement proposed by *Wilcock et al.* [1996] and *Wu and Chou* [2003]. Combined with *Wilcock and Crowe's* [2003] sediment transport equation and a gravel transfer function proposed by *Hoey and Ferguson* [1994] and *Toro-Escobar et al.* [1996], the proposed formulations were incorporated into The Unified Gravel-Sand (TUGS) model. The model is then applied to simulate three relatively large-scale flume experiments conducted at St. Anthony Falls Laboratory (SAFL) and reported by *Paola et al.* [1992], *Seal et al.* [1995, 1997], and *Toro-Escobar et al.* [1996]. Without any modification to the coefficients in the equation of *Wilcock and Crowe's* [2003], the model excellently reproduced the grain size distributions of the sediment deposits. The simulated bed slopes for all the three runs, however, are steeper than that observed in the experiments. Several attempts are made to improve the simulated bed slope, and it was found that replacing the dimensionless sediment transport \sim normalized shear stress relation in the *Wilcock and Crowe* [2003] equation (i.e., Equation (7) in the original reference) with a *Parker* [1990] type of relation matches both bed slopes and grain size distributions of the sediment deposit for all the three runs. This adjustment is considered to be minor, and the excellent match between simulation and observation with a minor adjustment indicate that the model is likely to be useful in simulating natural and management scenarios in

rivers. In order to explore the potential usefulness of the entrainment function, the flushing flow experiment of *Wu and Chou* [2003] is simulated and produced reasonable results compared with the observed data. In a manuscript submitted concomitantly with this manuscript [*Cui*, 2007], I examine model performance under field scale and provide comparisons of bed material fine sediment fractions under different hydrologic and sediment supply conditions.

2. Conceptual Three-Layer Model and Notations for Grain Size Distributions

[4] The conceptual model adapted in TUGS model is the widely used three-layer model [e.g., *Hirano*, 1971; *Ribberink*, 1987; *Parker*, 1990, 1991a, 1991b; *Parker and Sutherland*, 1990; *Wilcock and Crowe*, 2003; *Cui et al.*, 2003b, 2006a, 2006b; *Cui and Parker*, 2005; *Cui and Wilcox*, 2007]. According to this conceptual model, a sediment deposit in a gravel bedded river is composed of a surface layer (or active layer), which lies on top of the subsurface sediment (the second layer). A third bed load-layer is composed of the sediment particles transported as bed load over the surface layer. The three layers, along with the concept of the interface layer, are shown in Figure 1. For the simulation of channel bed dynamics, the interface layer was defined by previous researchers [e.g., *Hirano*, 1971; *Ribberink*, 1987; *Parker* 1991a, 1991b) as the layer of sediment to be deposited on top of the existing subsurface layer during aggradation (Figure 1a) and the layer of sediment to be released from the top of the subsurface layer during degradation (Figure 1b). That is, interface sediment becomes part of the subsurface layer following aggradation and was part of the subsurface layer prior to channel degradation. Note that the interface layer exists only conceptually because, given a time increment Δt , the thickness of the interface layer during this time increment approaches zero when $\Delta t \rightarrow 0$, and hence the conceptual model is conventionally named as a three-layer model instead of a four-layer model. The basic concept of the bed load, surface, subsurface, and interface layers will help the understanding of the surface-based bed load equation and the sediment exchange functions presented in detail below. The grain size distribution of the surface layer sediment will be part of the input variables for applying the *Wilcock and Crowe's* [2003] bed load equation. Here it is important to first introduce the notations that describe the grain size distributions in the four layers before the *Wilcock and Crowe's* [2003] equation and other relations are introduced.

[5] To describe the grain size distribution of a bulk of sediment, it is first divided into two classes: sediment coarser than 2 mm (gravel and coarser, which will be referred to as gravel hereafter), and sediment finer than 2 mm (sand and finer, which will be referred to as sand hereafter). For simplicity, it is assumed that there is no sorting within the sand class during its transport except that its fraction may vary at different locations and change in time. Thus the grain size distribution for the sand class can be simplified as a geometric mean grain size D_{gs} and a geometric standard deviation σ_{gs} , where the first subscript g denotes geometric and the second subscript s denotes sand. Procedures for calculating D_{gs} and σ_{gs} can be found in the

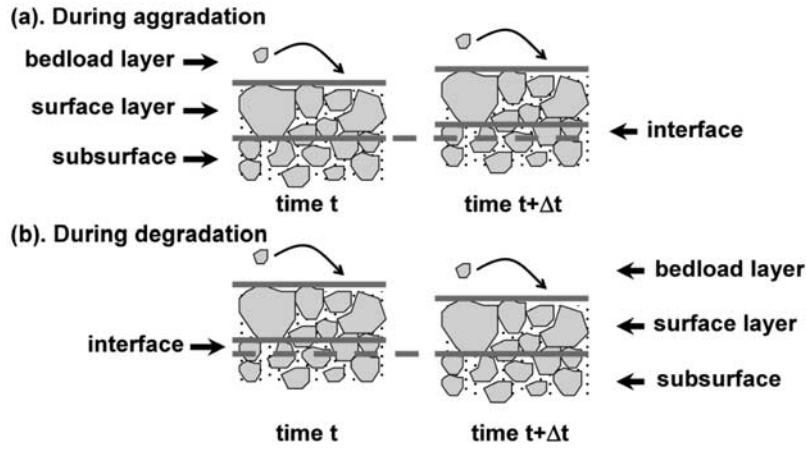


Figure 1. Conceptual three-layer model in a gravel bedded river [after *Parker 1991a, 1991b*], showing the bed load layer, the surface layer, and the subsurface layer. The interface sediment is the sediment that becomes part of the subsurface during aggradation (a) and the subsurface sediment to be eroded from the subsurface during degradation (b).

work of *Cui et al.* [1996]. The gravel class is divided into N groups bounded by $N + 1$ grain sizes, $D_1, D_2, \dots, D_N, D_{N+1}$, where D_1 is always 2 mm (i.e., the boundary between sand and gravel). The j -th size group, where j is between 1 and N , is bounded by grain size D_j and D_{j+1} with a mean grain size $\bar{D}_j = \sqrt{D_j D_{j+1}}$. The grain size distribution of the gravel class (i.e., the bulk sediment excludes sand and finer) is then represented with volumetric fractions of the N size groups. Knowing the fraction of sand within the bulk sample, and the fraction of each gravel size group within the gravel class, we will be able to define the grain size distribution of the combined gravel and sand. For example, we would describe the grain size distribution of the surface layer with sand fraction F_s , and the fractions of different gravel size groups within the gravel class, F_1, F_2, \dots, F_N , so that F_1, F_2, \dots, F_N sum to unity. It is important to note that the notation for grain size distributions used here is different from that by *Wilcock and Crowe* [2003] due to the simplification made to treat the entire sand class as one grain size group, and yet, to preserve its geometric mean and geometric standard deviation values. The above notation allows for more concise presentations of gravel and sand transfer functions (to be presented later) than if the notations of *Wilcock and Crowe* [2003] is adapted. The simplification of treating the entire sand class as a single bin is necessary because it significantly reduces the computer memory during simulation, thus allowing for storage of more sediment deposit layers. Because sand class is simplified as a single bin, the same geometric mean grain size (D_{gs}) and geometric standard deviation (σ_{gs}) apply to sand class in all the sediment used in the model (i.e., in bed load, surface layer, subsurface, and interface). Similar to the surface layer, where the fraction of sand and the fractions of different gravel size groups within the gravel class are denoted as $[F_s$ and $(F_1, F_2, \dots, F_N)]$, the fraction of sand and fractions of different gravel size groups within the gravel class for bed load, subsurface, and interface are denoted as $[p_s, (p_1, p_2,$

$\dots, p_N)]$, $[f_s, (f_1, f_2, \dots, f_N)]$, and $[f_{is}, (f_{i1}, f_{i2}, \dots, f_{iN})]$, respectively, where $\sum_{j=1}^N p_j = 1$, $\sum_{j=1}^N f_j = 1$, and $\sum_{j=1}^N f_{ij} = 1$.

3. Surface-Based Bed Load Equation for Combined Coarse and Fine Sediment [*Wilcock and Crowe, 2003*]

[6] TUGS model implements the surface-based bed load equation of *Wilcock and Crowe* [2003] for evaluation of bed load transport capacity. Here only a brief summary of the equation is provided to facilitate the discussions of the model, and its details can be found in the original reference [*Wilcock and Crowe, 2003*]. As pointed out earlier, some of the notations used in this paper are different from the original notations by *Wilcock and Crowe* [2003], and thus certain components of the *Wilcock and Crowe* [2003] equation given below may have a different form than the original reference. The *Wilcock and Crowe* [2003] equation adapted with the notations used in this paper is presented below:

$$W_j^* = \begin{cases} 0.002(\tau/\tau_{rj})^{7.5}, & \text{for } \tau/\tau_{rj} < 1.35 \\ 14(1 - 0.894/\sqrt{\tau/\tau_{rj}})^{4.5}, & \text{for } \tau/\tau_{rj} \geq 1.35 \end{cases}, \quad j = 1, 2, \dots, N, \text{ or } s \quad (1)$$

in which τ denotes bed shear stress, τ_{rs} and τ_{rj} ($j = 1, 2, \dots, N$) denote the reference shear stress for sand and for the j -th size group of the gravel class, respectively (to be discussed in more detail below), and W_s^* and W_j^* denote dimensionless transport rate for sand and for the j -th size group of the gravel class, as defined below:

$$W_s^* = \frac{RgQ_s}{Bu_*^3 F_s}, \quad (2a)$$

$$W_j^* = \frac{RgQ_{gj}}{Bu_*^3 (1 - F_s) F_j} \quad (2b)$$

in which R denotes submerged specific weight of sediment particles, g denotes gravitational acceleration, B denotes channel width (assuming a rectangular channel), u_* denotes shear velocity (and $u_* = \sqrt{\tau/\rho}$, where ρ denotes the density of water), Q_s denotes the volumetric transport rate for sand, and Q_{gj} denotes the volumetric transport rate for the j -th size group of the gravel class. The reference shear stresses, τ_{rs} and τ_{rj} , were defined by *Wilcock and Crowe* [2003] so the shear stress at which the dimensionless sediment transport rates, W_s^* and W_j^* , have a low value of 0.002, as indicated in equation (1). The reference shear stress, τ_{rs} and τ_{rj} , are grain size dependent:

$$\frac{\tau_{rs}}{\tau_{rsg}} = \left(\frac{D_{gs}}{D_{sg}} \right)^b, \quad (3a)$$

$$\frac{\tau_{rj}}{\tau_{rsg}} = \left(\frac{\bar{D}_j}{D_{sg}} \right)^b, \quad (3b)$$

$$b = \frac{0.67}{1 + \exp(1.5 - \bar{D}_j/D_{sg})} \quad (3c)$$

in which τ_{rsg} denotes a surface geometric mean based reference shear stress, and D_{sg} denotes the geometric mean grain size of the surface layer (including both sand and gravel classes). On the basis of flume experimental data, *Wilcock and Crowe* [2003] proposed that surface geometric mean based reference shear stress, τ_{rsg} , decreases with the increase in surface sand fraction (F_s):

$$\frac{\tau_{rsg}}{\rho R g D_{sg}} = 0.21 + 0.15 \exp(-20F_s) \quad (4)$$

The above equations allow for the calculation of the transport rates of sand (Q_s) and gravel at each size group (Q_{gj}), and from which, to calculate the overall gravel transport rate (Q_g) and the bed load grain size distribution as expressed with values of $p_s, p_1, p_2, \dots, p_N$:

$$Q_g = \sum_{j=1}^N Q_{gj}, \quad (5a)$$

$$p_s = \frac{Q_s}{Q_s + Q_g}, \quad (5b)$$

$$\text{and } p_j = \frac{Q_{gj}}{Q_g} \quad (5c)$$

4. Linking Grain Size Distributions of the Subsurface Sediment Deposit With the Surface Layer

[7] The *Wilcock and Crowe's* [2003] equation does not provide a direct link between grain size distributions in the bed load and the surface layer with that in the subsurface.

Before the *Wilcock and Crowe's* [2003] equation can be implemented into a numerical model, a linkage between the bed load, surface layer and subsurface grain size distributions needs to be established.

[8] The transfer of sediment among the bed load, surface layer and subsurface are discussed for cases of bed degradation and bed aggradation below. In the case of bed degradation, it has been recognized since the work of *Hirano* [1971] that the surface layer mines the subsurface (Figure 1b), and thus,

$$f_{ij} = f_j; \quad (6a)$$

$$\text{and } f_{is} = f_s \quad (6b)$$

Equation (6a) has been used for simulation of bed degradation in all the Parker family of models [e.g., *Parker, 1991a, 1991b; Cui et al., 1996, 2003b, 2006a, 2006b; Cui and Parker, 2005; Cui and Wilcox, 2007*]. Note that Equation (6b) implies that fine sediment in the deposit cannot be entrained unless the bed is eroded. Flume observations, however, indicate that, although fine sediment in the deposit cannot be entrained while the surface layer is static, it can be entrained to a depth of up to 2 to 3 surface layer thickness once the surface layer is mobilized [e.g., *Diplas and Parker, 1985*]. The entrainment of fine sediment without bed scouring is discussed further following the discussion of gravel and sand transfer functions in cases of bed aggradation below.

[9] In case of bed aggradation, *Cui and Parker* [2005] and *Cui et al.* [2003b, 2006a, 2006b] all applied the formulation proposed by *Hoey and Ferguson* [1994]:

$$f_{ij} = \chi p_j + (1 - \chi) F_j \quad (7)$$

in which $\chi = 0.7$ was derived based on the St. Anthony Falls Laboratory (SAFL) downstream fining experiment Run 3 by *Toro-Escobar et al.* [1996]. It should be noted that *Toro-Escobar et al.* [1996] excluded sediment particles finer than 2 mm from their analysis because the sand fraction data cannot collapse to the same relation as the gravel class sediments. With that, Equation (7), which, together with Equation (6a), will be referred to as gravel transfer function hereafter, will be implemented to TUGS model for the gravel class sediment. Here it is important to reiterate that interface sediment is the sediment that works into the subsurface layer during bed aggradation (Figure 1a) or to be released from the subsurface during bed degradation (Figure 1b). That is, any given layer of subsurface sediment is the integration of the interface sediment over a period of time during which this particular layer of subsurface sediment was deposited, and thus, subsurface sediment samples can be used as a surrogate of interface sediment in deriving sediment transfer functions [e.g., *Toro-Escobar et al., 1996*]. Similar to the practice of *Toro-Escobar et al.* [1996], subsurface sediment samples will be used as surrogates for interface sediment when a hypothetical sand

transfer function for the case of bed aggradation is compared with field data below.

[10] To simplify the sand transfer relation, bed load sand fraction is dropped out of the relation, and only the fractions of sand in the surface layer and interface are considered. Because the surface and bed load sand fractions are strongly correlated, as suggested by the *Wilcock and Crowe* [2003] equation, linking the subsurface sand fraction only to the surface sand fraction implicitly links the subsurface sand fraction to the bed load sand fraction. The following considerations and constraints are taken into account in formulating a hypothetical sand transfer function during channel aggradation: (1) The interface sediment sand fraction should increase as the surface sand fraction increases; (2) the interface sediment sand fraction should decrease with the increase in the geometric standard deviation of the gravel class of the interface sediment, because a higher geometric standard deviation implies less matrix space left for sand deposition [*Cui and Parker, 1998*]; (3) the sand fraction in the interface sediment should be equal to or higher than surface sand fraction because the subsurface sediment should generally be finer than that in the surface layer; and (4) the calculated range of the interface sand fractions should generally fall within the same range as the subsurface sand fractions measured in the field. The proposed hypothetical sand transfer function during bed aggradation is written as

$$f_{is} = \begin{cases} 0.4 - 0.1\sigma_{gg} + (0.6 + 0.1\sigma_{gg})F_s, & \text{for } \sigma_{gg} < 4 \\ F_s, & \text{for } \sigma_{gg} \geq 4. \end{cases} \quad (8)$$

in which σ_{gg} denotes geometric standard deviation of the gravel class of the interface sediment. Equation (8) is constructed so that it satisfies the four considerations and constraints discussed earlier. In addition, f_{is} approaches to unit as F_s increases to unity. Note that $f_{is} \neq 0$ when $F_s = 0$, which seems to be a violation of the physical principle that no sand should be deposited into the subsurface if there is no sand in transport (indicated with $F_s = 0$). While it is seemingly the case, the physical principle is guaranteed in the mass conservation calculation in the simulation, in which the rate of fine sediment deposition cannot exceed the rate of sediment transport at the upstream node, thus satisfying the condition that $f_{is} = 0$ when $F_s = 0$. The threshold of $\sigma_{gg} = 4$ in Equation (8) is chosen so that it satisfies $f_{is} \geq F_s$. As a matter of fact, very rarely the geometric standard deviation of the gravel portion of a sediment deposit exceeds 4. The predicted interface sand fraction with the hypothetical sand transfer function (Equation (8)) for different gravel geometric standard deviations are shown in Figure 2, in comparison with field measurements of subsurface sand fractions. Figure 2a shows that the interface sand fraction increases with the increase in surface sand fraction and decreases with the increase in gravel geometric standard deviation. In addition, the field measurements of subsurface sand fractions fall in the general range of the predicted interface sand fractions. In Figure 2b, interface sand fractions are calculated based on the observed surface sand fractions and subsurface gravel geometric standard deviations, and compared with mea-

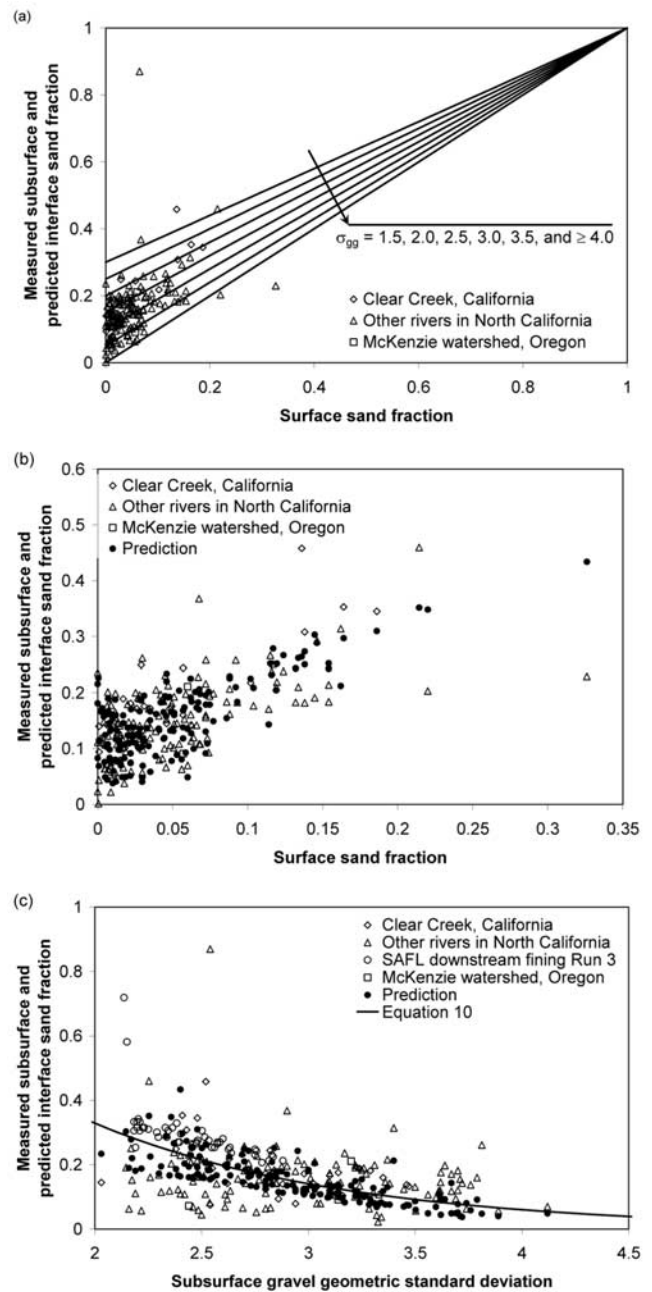


Figure 2. Hypothetical sand transfer function during aggradation, compared with field and flume data for surface/subsurface sand fractions. (a) hypothetical relation under different subsurface geometric mean standard deviations, in comparison with field data; (b) calculated interface sand fraction presented as a function of surface sand fraction, in comparison with field measurement of subsurface sand fractions; (c) calculated interface sand fraction presented as a function of subsurface gravel standard deviation, in comparison with field measurements of subsurface sand fractions. Data source: Clear Creek: Matt Brown, Jess Newton, *Graham Matthews and Associates* [2003a, 2004]; other rivers in North California (Sacramento, Trinity, Stanislaus, Tuolumne, and tributaries to Trinity): *Graham Matthews and Associates* [2001, 2003b], Geoff Hales, *CDWR* [1994, 1995]; McKenzie watershed: John Wooster (unpublished data).

sured subsurface sand fractions. The comparison shows that the calculated interface sand fractions and measured subsurface sand fractions generally fall into the same range. Figure 2c shows the same data as Figure 2b, except that they are presented as a function of gravel geometric standard deviation, showing the decreasing interface/subsurface sand fraction with increasing gravel geometric standard deviation.

5. Entrainment and Infiltration of Fine Sediment From/Into the Subsurface

[11] The gravel and sand transfer functions discussed above simulate the co-erosion and co-deposition of gravel and sand in case of bed degradation and aggradation. Fine sediment within the deposit, however, can be entrained for up to a depth of two to three times of the surface layer thickness without bed scouring and redeposition once the surface layer is mobilized [*Diplas and Parker, 1985*] in the absence of bed aggradation and degradation. In addition, a sediment deposit that does not have enough fine sediment in its pores (e.g., shortly after a flushing flow event) will allow fine sediment to infiltrate back into the subsurface, if fine sediment is available in bed load or suspended load. Many flume experiments have suggested that the infiltration depth is usually a few surface layer thicknesses [e.g., *Beschta and Jackson, 1979; Diplas and Parker, 1985*], which is similar to the depth of fine sediment entrainment. In the absence of physically based equations to describe the entrainment and infiltration of fine sediment from and into the subsurface deposits, hypothetical relations based on the concept of *Wilcock et al. [1996]* and *Wu and Chou [2003]* are proposed below and implemented in the model. Before introducing the hypothetical relations, the concepts for equilibrium surface sand fraction for sand entrainment (F_{se}) and equilibrium subsurface sand fraction for sand infiltration (f_{se}) are introduced. The equilibrium surface sand fraction for sand entrainment is a surface sand fraction value, above which no subsurface sand will be entrained. If Equation (8) is considered as an equilibrium relation between surface sand fraction and subsurface sand fraction, it can be reversed to come up with the equilibrium surface sand fraction for sand entrainment by replacing interface sand fraction f_{is} with subsurface sand fraction f_s :

$$F_{se} = \begin{cases} (f_s + 0.1\sigma_{gg} - 0.4)/(0.6 + 0.1\sigma_{gg}), & \text{for } \sigma_{gg} < 4 \\ f_s, & \text{for } \sigma_{gg} \geq 4 \end{cases} \quad (9)$$

The equilibrium subsurface sand fraction for sand infiltration is a subsurface sand fraction, above which no sand will be able to infiltrate into the subsurface deposit. Note that subsurface sand fraction can be higher than this equilibrium subsurface sand fraction through co-deposition of gravel and sand, realized through the implementation of Equation (8) in the numerical model. The equilibrium subsurface sand fraction for sand infiltration is defined based on visual fitting of field and laboratory data shown in Figure 2c, and is given below:

$$f_{se} = 1.8 \exp(-0.85\sigma_{gg}) \quad (10)$$

The sand entrainment and infiltration fluxes per unit area are then hypothesized as:

$$q_e = \begin{cases} \frac{a_e u_*^3}{RgD_{sg}} W_i^* (\tau/\tau_{rsg})(F_{se} - F_s), & \text{for } F_s < F_{se} \\ 0, & \text{for } F_s \geq F_{se}. \end{cases} \quad (11a)$$

$$q_i = \begin{cases} \frac{a_i v_s^3}{RgD_{sg}} F_s (f_{se} - f_s), & \text{for } f_s < f_{se} \\ 0, & \text{for } f_s \geq f_{se} \end{cases} \quad (11b)$$

in which q_e and q_i denote sand entrainment and infiltration fluxes per unit area, respectively; v_s denotes settling velocity, and a_e and a_i are dimensionless coefficients that must be assigned through model calibration. Note that both q_e and q_i have units of velocity. The term $(a_e u_*^3)/(RgD_{sg})$ in Equation (11a) is proposed in analogy to the sediment transport equations of *Parker [1990]* and *Wilcock and Crowe [2003]*, and in Equation (11b) shear velocity u_* is replaced with settling velocity v_s . The implication of Equation (11a) is that the rate of entrainment is proportional to sand transport rate and proportional to the deviation of surface sand fraction from its equilibrium value. The implication of Equation (11b) is that the rate of fine sediment infiltration is proportional to surface fine sediment fraction and the deviation of subsurface sand fraction from its equilibrium value. An overall vertical sand transport rate per unit channel area, q_{sv} , can be calculated by combining the fluxes of entrainment and infiltration:

$$q_{sv} = q_e - q_i \quad (12)$$

Note that q_{sv} can be either positive or negative. A positive q_{sv} value indicates a net upward sand flux (i.e., entrainment) and a negative q_{sv} value indicates a net downward sand flux (i.e., infiltration).

[12] It is important to reiterate that the concepts used in Equations (11a) and (11b) in this section are hypothetical, and can only be used with adequate model calibration. The equations, however, can be conveniently replaced with better ones once they are available. In addition, fine sediment infiltration and entrainment into/from subsurface can be assumed to cancel off each other for long-term simulations of natural rivers (i.e., by setting $a_i = 0$ and $a_e = 0$). For the moment, they are implemented in TUGS model for exploratory purposes. Later in this paper the flushing flow data of *Wu and Chou [2003]* are used to demonstrate that the entrainment function, calibrated to a specific problem, can produce reasonable results.

6. Governing Equation for Water Flow

[13] The governing equations for water flow used in this model are identical to that in *Cui et al. [2006a, 2006b]*, and are briefly presented below. To be able to simulate both sub- and supercritical flow conditions, the backwater equation is employed for low Froude number conditions and quasi-

normal flow assumption is applied for high Froude number flow conditions.

$$\begin{cases} \frac{dh}{dx} = \frac{S_0 - S_f}{1 - F_r^2}, & F_r \leq F_{rn} \\ S_f = S_0, & F_r > F_{rn} \end{cases} \quad (13)$$

in which h denotes water depth; x denotes downstream distance, S_0 denotes local bed slope; S_f denotes friction slope; and F_r denotes Froude number, which is calculated by assuming a wide rectangular channel:

$$F_r = \frac{Q_w}{Bh\sqrt{gh}} \quad (14)$$

in which Q_w denotes water discharge; B denotes channel width, which is generally chosen as bankfull width and assumed to be a function of location but does not change in time; and g denotes acceleration of gravity. F_{rn} in Equation (13) is the critical Froude number that separates the application of backwater equation and quasi-normal flow assumption. Here an arbitrary value of $F_{rn} = 0.8$ is used in the simulation, and any F_{rn} value of between 0.75 and 0.9 produces similar results. The friction slope S_f is calculated with the Keulegan formulation below,

$$\frac{Q_w}{Bh\sqrt{ghS_f}} = 2.5 \ln\left(11 \frac{h}{k_s}\right) \quad (15a)$$

in which k_s denotes roughness height and is assumed to be proportional to surface layer geometric mean grain size of combined gravel and sand,

$$k_s = 2.5D_{sg} = 2.5D_{gs}^{F_s}D_{sgg}^{1-F_s} \quad (15b)$$

in which D_{sg} denotes the geometric mean grain size of the surface layer for combined gravel and sand; and D_{sgg} denotes the surface gravel geometric mean grain size. Because k_s is located inside the log function in Equation (15a), a specific choice of a k_s value is not particularly sensitive to model simulation. Here in Equation (15b) k_s is assumed to be 2.5 times of the surface geometric mean grain size as it produces reasonable results as demonstrated later in this paper. Because the model is designed primarily for simulation of gravel bedded rivers, and also for simplicity, form friction is assumed to be relatively unimportant and is ignored in the current model. Form friction may become important once both surface and subsurface become predominantly sandy, allowing for easier formation of bed forms (e.g., dunes, anti-dunes).

[14] Combining the backwater equation and quasi-normal flow assumption under different Froude number flow conditions allows for a relatively simple algorithm in simulating sub- and supercritical flow conditions, and the results from the simulation are almost identical to more complicated methods [e.g., *Cui et al.*, 1996, 2005, and *Cui and Parker*, 1997] as demonstrated by *Cui et al.* [2005], and *Cui et al.* [1996].

7. The Exner Equations of Sediment Continuity

[15] The Exner equations of sediment continuity are modified from those by *Parker* [1991a, 1991b] to include

the presence of sand, and differ from those by *Cui et al.* [2006a, 2006b] in that *Cui et al.* [2006a, 2006b] considered gravel to form the frame of the deposit as the channel aggrades, while sand only fills into the pores of the gravel deposit. The current model considers both gravel and sand as the matrix of the deposit. It is useful to point out that the Exner equations of sediment continuity is explained only briefly in this paper due to space limitations. The equations, however, are similar to those by *Parker* [1991a, 1991b], *Cui and Parker* [1998, 2005], and *Cui et al.* [2003b, 2006a, 2006b] in many ways. In particular, the equations presented by *Cui et al.* [2006a, 2006b] are discussed in detail by *Stillwater Sciences* [2002], which should provide adequate information for interested readers to fully understand the different components in the equations presented below. The Exner equations for sediment continuity are:

$$(1 - \lambda_p)B \frac{\partial \eta}{\partial t} + \frac{\partial(Q_g + Q_s)}{\partial x} + (2 - F_s)\beta_a Q_g = q_{gl} + q_{sl} \quad (16a)$$

$$\begin{aligned} (1 - \lambda_p)B \left(\frac{\partial[(1 - F_s)L_a F_j]}{\partial t} + (1 - f_{ls})f_{lj} \frac{\partial(\eta - L_a)}{\partial t} \right) \\ + \frac{\partial(Q_g p_j)}{\partial x} + \beta_a Q_g [p_j + (1 - F_s)F_j^j] \\ + \frac{\beta_a Q_g}{3\ell n(2)} \left(\frac{p_j + (1 - F_s)F_j^j}{\psi_{j+1} - \psi_j} - \frac{p_{j+1} + (1 - F_s)F_{j+1}^j}{\psi_{j+2} - \psi_{j+1}} \right) = q_{glj} \end{aligned} \quad (16b)$$

$$\begin{aligned} (1 - \lambda_p)B \left(\frac{\partial(F_s L_a)}{\partial t} + f_{ls} \frac{\partial(\eta - L_a)}{\partial t} \right) \\ + \frac{\partial Q_s}{\partial x} - \frac{\beta_a Q_g}{3\ell n(2)} \frac{p_1 + (1 - F_s)F_1^j}{\psi_2 - \psi_1} = q_{sl} \end{aligned} \quad (16c)$$

in which λ_p denotes porosity of the sediment deposit; η denotes the thickness of sediment deposit; t denotes time, β_a denotes volumetric abrasion coefficient (fraction of volume lost per unit distance transported); q_{gl} and q_{sl} denote lateral gravel and sand input rates per unit distance (e.g., from bank erosion or tributaries); L_a denotes surface layer thickness; p_j denotes fraction of the j -th size group of the gravel class of the bed load (and p_1 is for $j = 1$); F_j^j is an areal estimate of the fraction of exposure of surface gravel of the j -th group (and F_1^j is for $j = 1$) given by *Parker* [1991a, 1991b] below:

$$F_j^j = \frac{F_j / \sqrt{D_j}}{\sum (F_j / \sqrt{D_j})} \quad (17)$$

q_{glj} denotes the lateral gravel input rate per unit distance for the j -th size group, so that $\sum q_{glj} = q_{gl}$; and ψ_j denotes base-2 logarithmic grain size psi-scale associated with grain size D_j , i.e.,

$$\psi_j = \log_2(D_j), \quad j = 1, 2, \dots, N, N + 1 \quad (18)$$

Equation (16a) is the conservation of total sediment load (sand and gravel), in which the last term on the left hand

side is a sink term, representing gravel loss to silt as gravel abrades into smaller gravel particles, sand, and silt [Parker, 1991a, 1991b]. No sink term for sand is present in Equation (16a) because the equation considers the mass conservation for combined gravel and sand. Equation (16b) is the conservation of gravel in the j -th size group, in which the first term involving β_a represents gravel mass lost to silt by abrasion and the second term involving β_a represents gravel mass transfer between adjacent size groups through abrasion. The factor $(1 - F_s)$ in the abrasion term is the result that only $(1 - F_s)$ of the surface layer is composed of gravel, and the factor $(2 - F_s)$ in Equation (16a) is the result of $\Sigma[p_j + (1 - F_s)F_j']$. Equation (16c) is the conservation of sand, in which the last term on the left hand side represents increased sand mass through abrasion of gravel, which is also seen in Equation (16b) for the finest gravel size group (i.e., for $j = 1$).

[16] For simplicity, the hypothetical sand entrainment and infiltration relations are not included in the Exner equations of sediment continuity (Equations (16a), (16b), and (16c)). Instead, a relatively simple procedure is used to re-update the subsurface sand fraction and adjust sand transport rate following the solution of the Exner equations above, once sand entrainment or infiltration occurs. At each step, the subsurface sand fraction is updated as

$$f_s = f'_s - \frac{q_{vs}\Delta t}{(1 - \lambda_p)H_{ei}} \quad (19)$$

in which f'_s denotes the subsurface sand fraction calculated without considering sand entrainment and infiltration; Δt denotes time increment; and H_{ei} denote the depth of the subsurface that subjects to entrainment and infiltration. The addition or reduction of sand transport rate through sand entrainment or infiltration is then factored into the overall mass balance with:

$$q_{sl} = q'_{sl} + q_{sv}B \quad (20)$$

in which q'_{sl} denotes lateral sediment input, shown in Equations (16a) and (16c) as q_{sl} . In addition to the adjustment of f_s and q_{sl} due to sand entrainment and infiltration, porosity λ_p is adjusted by replacing the entrained sand with porous space for entrainment and replacing the porous space with sand for infiltration. According to this, the following formulation can be used to adjust the porosity whenever subsurface sand entrainment or infiltration occurs:

$$f_s + \frac{\lambda_p}{1 - \lambda_p} = f'_s + \frac{\lambda'_p}{1 - \lambda'_p} \quad (21)$$

in which λ'_p denotes porosity before adjustment and λ_p denotes porosity after adjustment.

8. Brief Description of Solution Procedure

[17] The sediment transport equation of *Wilcock and Crowe* [2003] (Equations (1) through (5)), gravel transfer functions (Equations (6a) and (7)), sand transfer functions (Equations (6b) and (8)), sand entrainment and infiltration functions (Equations (9), (10), (11a), (11b), and (12)), governing equation for flow (Equation (13)), friction for-

mulation (Equation (15a)), and the Exner equations of sediment continuity (Equations (16a), (16b), (16c), (19), and (20)) are organized and solved with FORTRAN program language to form The Unified Gravel-Sand (*TUGS*) Model. A brief procedure for the solution is provided below.

[18] Note the partial differential equations (PDE) are discretized as first order accurate both in space and in time; the discretization in time is explicit, and the spatial discretization is conducted with the standard upwind scheme [e.g., *Hirsch*, 1989]. The PDEs indicated in the following brief description of solution procedure all refers to their discretized form.

[19] • Solve the backwater equations and resistance (friction) relations, Equations (13), (14), (15a), and (15b) based on the information at time t ;

[20] • Calculate gravel and sand transport rates and bed load grain size distribution with *Wilcock and Crowe* [2003] equation, Equations (1), (2a), (2b), (3a), (3b), (3c), (4), and (5a), (5b), (5c);

[21] • Solve Equation (16a) to determine the amount of aggradation or degradation between time t and $t + \Delta t$;

[22] • Calculate interface sediment grain size distribution as represented with parameters $f_{1s}, f_{11}, f_{12}, \dots, f_{1N}$ with Equations (6a), (6b), or (7) and (8), depending on whether the bed is degrading or aggrading;

[23] • Solve Equations (16b) and (16c) to update surface grain size distribution as represented by parameters $F_s, F_1, F_2, \dots, F_N$;

[24] • In case of aggradation, update subsurface sediment grain size distribution by mixing the interface sediment with the top layer of the subsurface sediment (details not presented but the mixing is a linear combination and is very simple to implement);

[25] • Adjust f_s, q_{sl} , and λ_p for sand entrainment and infiltration with Equations (9), (10), (11a), (11b), (12), (19), (20), and (21);

[26] • Update all the record for time $t + \Delta t$ and go to the next time step.

9. Simulating SAFL Downstream Fining Flume Runs

[27] Model performance is examined with three SAFL downstream fining narrow flume runs [*Paola et al.*, 1992; *Seal et al.*, 1995, 1997; *Toro-Escobar et al.*, 1996]. The three experimental runs were conducted in a 0.305-m wide and 50-m long flume with an initial concrete-bottom slope of 0.002 (Figure 3). The grain size distribution of the sediment used to feed the flume is shown in Figure 4, which is 33.1% sand and 66.9% gravel, and has a geometric mean grain size of 4.63 mm and a geometric standard deviation of 5.57 [*Cui et al.*, 1996]. Each of the three runs is conducted with a constant water discharge and a constant sediment feed rate. The flume is ponded at its downstream reach by setting a constant water surface elevation at the downstream end, which drives channel aggradation and downstream fining. The relevant parameters for the three runs are given in Table 1. During the experiments, channel bed elevations were monitored at several intervals. Samples of the sediment deposits were then collected and analyzed following the termination of each run. The samples were taken in layers and were labeled with the duration the layer of sediment was deposited (e.g., 5–10 h denotes the layer of

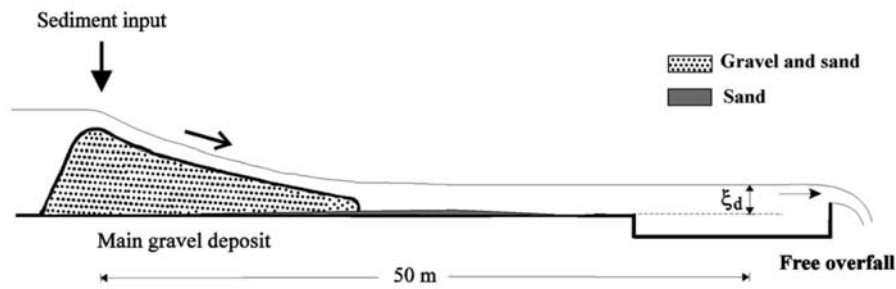


Figure 3. Flume set up for SAFL downstream fining experiments.

sediment that was deposited between 5 and 10 h). Full description of the experimental data is given by Seal *et al.* [1995].

[28] Three previous numerical simulations had been conducted by this author and his co-contributors to simulate the three SAFL downstream fining experiments [i.e., Cui *et al.*, 1996, 2006b; Cui and Parker, 1997]. Parker's surface-based bed load equation had been used in all these three previous efforts. Among other things, the major differences in the three previous simulations are in the methods used to solve the flow parameters. In the simulation of Cui *et al.* [1996], a time-relaxation method was used to solve the non-steady flow equations in order to reach a steady flow solution for the transient flow, which is a rather inefficient solution by today's standards. In the simulation of Cui and Parker [1997], a shock-fitting method was used to capture the precise position of the sediment wedge front and hydraulic jump so that a quasi-normal flow assumption could be applied upstream of the hydraulic jump while a simple backwater calculation was used downstream of the hydraulic jump. Because of the good results of Cui and Parker [1997], Cui *et al.* [2003a] and Cui and Parker [2005] simplified the procedure and started to calculate flow parameters with a combination of quasi-normal flow assumption for high Froude number reaches and simple backwater calculation for low Froude number reaches, and Cui *et al.* [2006b] simulated the SAFL downstream fining

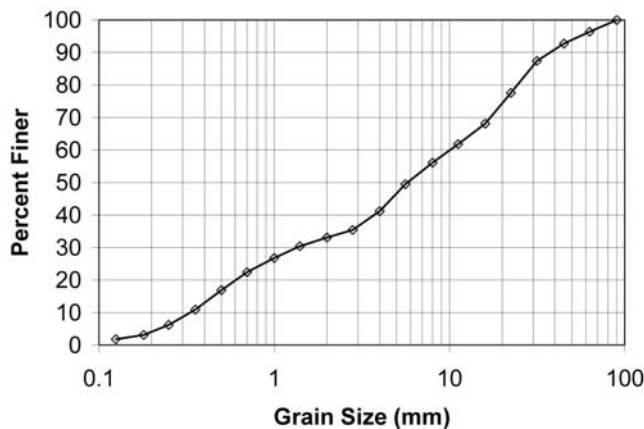


Figure 4. Grain size distribution of the sediment used for sediment feed in the three narrow runs of SAFL downstream fining experiments.

Run 2 with this simplified method to demonstrate that it produced almost identical results compared with that in Cui *et al.* [1996] and Cui and Parker [1997]. This simplified method is also used in TUGS model presented in this paper and by Cui and Wilcox [2007]. Because Parker's [1990] equation excludes sand from the simulation, the previous efforts of Cui *et al.* [1996, 2006b] and Cui and Parker [1997] for the SAFL downstream fining runs did not simulate fraction of sand in the deposit, whereas the TUGS simulation presented below simulates the fraction of sand in the deposit in addition to the previously simulated bed profile and gravel characteristic grain sizes, and compares the results with experimental observations.

9.1. TUGS Model Simulation With Unmodified Wilcock and Crowe [2003] Equation

[29] Because the SAFL experimental runs applied constant water discharge and sediment feed, the gravel and sand are co-deposited gradually onto the flume bed and there is no additional sand infiltration and entrainment. With that, parameter a_i and a_e were both set to zero for the numerical simulation (and because of this, the value of H_{ci} is irrelevant to this simulation, and porosity λ_p becomes a constant). The porosity λ_p is set to a constant value of 0.3 for the simulation, which is a typical value for deposits of gravel sand mixtures [e.g., Wu and Wang, 2006]. Because the experiment is conducted in a flume with a length of less than 50 m, particle abrasion is negligible, and thus, abrasion coefficient β_a is set to zero. Also, because there was no lateral input of sediment, parameters q_{gl} and q_{sl} are set to zero. Active layer thickness is set to a constant value of 5 cm, which is slightly larger than the D_{90} (i.e., the grain size that 90% of the sediment is finer than) of the feed sediment. Cui *et al.* [2006a] had demonstrated that the selection of

Table 1. Relevant Parameters in SAFL Downstream Fining Experiments, Narrow Runs

Run	1	2	3
Water discharge, l/s	49	49	49
Sediment feed rate, kg/min	11.30	5.65	2.83
Adjusted sediment feed rate, ^a kg/min	11.24	5.33	2.78
Experimental duration, h	16.83	32.4	64
Downstream end water surface elevation, m	0.40	0.45	0.50

^aSediment feed rates were adjusted to account for the sediment that rolled backward following sediment feed, as illustrated in Figure 3 [Cui *et al.*, 1996].

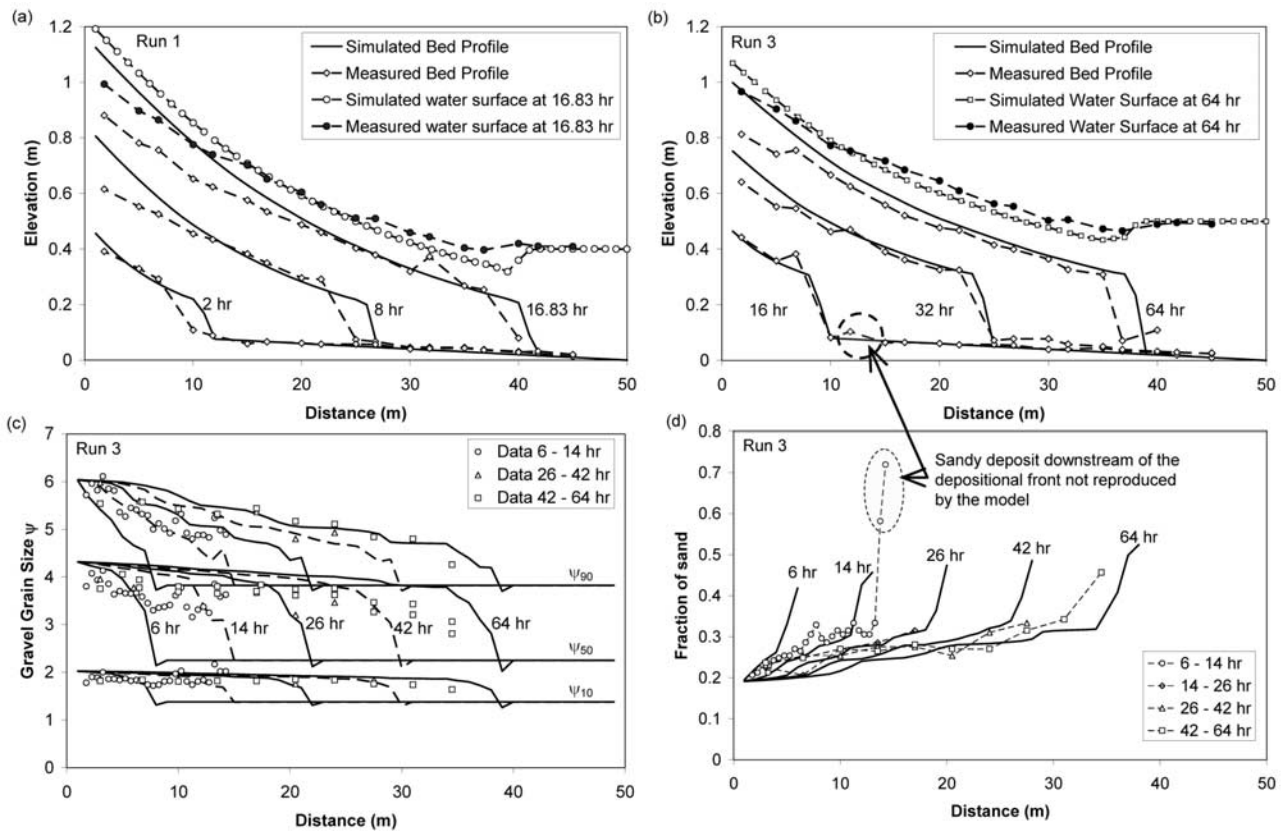


Figure 5. Simulated results with TUGS model, unmodified *Wilcock and Crowe* [2003] equation, in comparison with observations from flume measurements: (a) bed elevation for Run 1; (b) bed elevation for Run 3; (c) gravel characteristic grain sizes for Run 3, and (d) sand fraction in the deposit for Run 3. In (c), the lines are predicted results, alternating between solid and dashed lines at different times for better visualization.

active layer thickness is not particularly sensitive to modeling results, as long as it is within a reasonable range. The first attempt is made to simulate the three flume runs with the unadjusted TUGS model, i.e., no adjustment is made to the coefficients in *Wilcock and Crowe's* [2003] equation. Model results are shown in Figures 5a and 5b for bed elevations for Runs 1 and 3, respectively, in Figure 5c for gravel characteristic grain sizes in the deposits for Run 3, and in Figure 5d for sand fractions in the deposits for Run 3. Results in Figure 5 indicate that TUGS model, without any modification to *Wilcock and Crowe's* [2003] equation, excellently reproduced the grain size distributions of the sediment deposit, as indicated in the comparison of gravel characteristic grain sizes and sand fractions in the deposit (Figures 5c and 5d). The simulated gravel characteristic grain sizes (ψ_{10} , ψ_{50} , and ψ_{90}) shown in Figure 5c, for example, (a) closely match the observed values; (b) decrease in the downstream direction similar to observed in the flume; and (c) gradually increase in time to approach their equilibrium values (i.e., the values at $x = 0$). The simulated sand fractions shown in Figure 5d also closely match the observed values and the trend both in space and in time with the exception that there are two exceptionally high sand fraction values for the time interval between 6 and 14 h in the experiment that is not reproduced in the simulation. The observed two high sand fraction values

are samples from a small amount of sand deposit downstream of the main depositional front, as indicated in Figures 5b and 5d. During the experiment, as the majority of the gravel and sand is deposited as a sediment wedge that gradually build upward with its front gradually migrated downstream, a small amount of sand transported passed the depositional front, forming a small amount of sand deposit that were later buried by the main deposit as the front migrated downstream. This small amount of sand that passed the depositional front is not produced in this simulation. Simulation results for bed elevation indicate that the model over-predicted bed slope for all the three runs, as shown for Runs 1 and 3 in Figures 5a and 5b, and the simulated slope is more accurate as sediment feed rate decreases (i.e., Run 3 is better than Run 2, and Run 2 is better than Run 1). This observation indicates that some minor adjustments to the *Wilcock and Crowe* [2003] equation that increase its predicted sediment transport rate, particularly when shear stress is high, should allow for a better prediction of bed slope. The simulated volume of sediment deposit seems to be higher than the experimental data as shown in Figures 5a and 5b. One of the concerns is that a programming error had resulted in over predicted sediment mass in the simulation. To make sure that the numerical model conserves mass, a hand check of deposi-

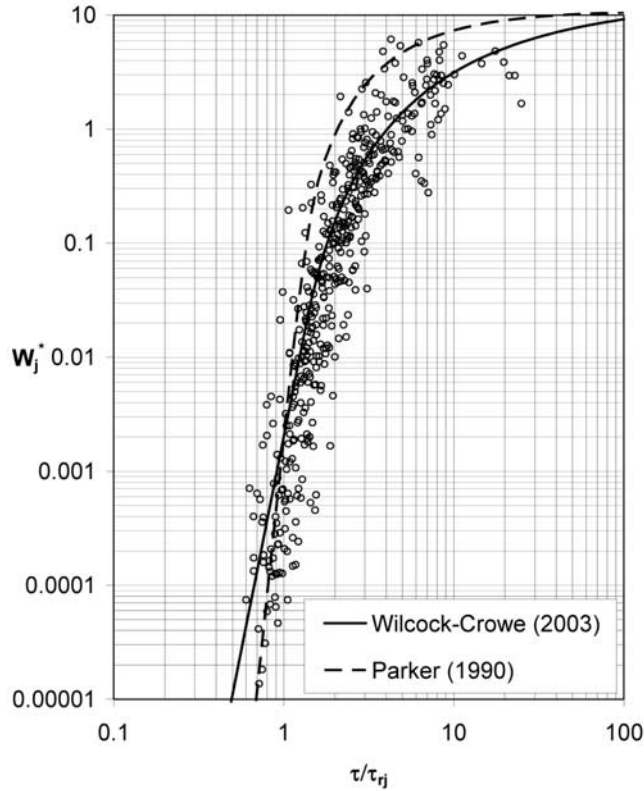


Figure 6. Dimensionless sediment transport rate \sim normalized shear stress relation. Experimental data are analyzed by applying Manning-Strickler resistance equation and water continuity equation to calculate water depth and shear stress. Data used for analysis come from the original data set of *Wilcock and Crowe* [2003] downloaded from <ftp://agu.org> under subdirectory 2001WR000683 in June 2006. The dimensionless sediment transport rate \sim normalized shear stress relations of both *Parker's* [1990] and *Wilcock and Crowe's* [2003] are presented with the data.

tional volume is conducted and it was confirmed that $\int_0^t (Q_g + Q_s) dt$ is almost identical to $[(1 - \lambda_p) \int_0^L \eta dx]_{\text{at time } t}$, where L denotes flume length. That is, the numerical simulation satisfies mass conservation. Another possibility is that the porosity value used in the simulation, $\lambda_p = 0.3$, is higher

$$W_j^* = \begin{cases} 10.95 \left(1 - \frac{0.853}{\tau/\tau_{ij}}\right)^{4.5}, & \text{for } \tau/\tau_{ij} > 1.59 \\ 0.002 \exp \left[14.2(\tau/\tau_{ij} - 1) - 9.28(\tau/\tau_{ij} - 1)^2 \right], & \text{for } 1 < \tau/\tau_{ij} \leq 1.59 \\ 0.002(\tau/\tau_{ij})^{14.2}, & \text{for } \tau/\tau_{ij} \leq 1 \end{cases} \quad (22)$$

than the porosity of the sediment deposit in the flume. The newly deposited sediment with a grain size distribution used in the experiment, however, rarely has a porosity value below 0.3, as indicated by the equations of *Komura* [1963] and *Han et al.* [1981], and both equations can be found in *Wu and Wang* [2006]. With that, the porosity value should

not be arbitrarily reduced to below 0.3 without any porosity measurements during the experiment. The most likely reason for the smaller sediment deposit volume than the simulation is that some fine sediment passed the depositional front and cannot be counted for in the bed profile comparison. In addition, potential deviation from the designed sediment feed during the flume experiments is also a possibility because sediment of the size (up to 90 mm in diameter) used in the experiments cannot be fed with a relatively accurate sediment feeder. The implication of the over predicted volume of sediment deposition will be discussed later following a revised simulation.

9.2. TUGS Model Simulation With Slightly Modified *Wilcock and Crowe* (2003) Equation

[30] Because the numerical model over predicted the bed slope, and the discrepancy between numerical simulation and flume experiment increases with the increase in sediment transport rate, an increase in the calculated sediment transport rate and an increase in the slope of the $W_j^* \sim \tau/\tau_{ij}$ relation (Equation (1)) of the *Wilcock and Crowe* [2003] equation will improve the numerical prediction. Here the sediment transport data collected by *Wilcock and Crowe* [2003] and used to derive their bed load equation are plotted in Figure 6, along with their $W_j^* \sim \tau/\tau_{ij}$ relation (the data are downloaded from <ftp://agu.org> under subdirectory 2001WR000683 in June 2006). In addition, the $W_j^* \sim \tau/\tau_{ij}$ relation of *Parker* [1990] is also plotted in the diagram for comparison purposes. For those who are familiar with *Wilcock and Crowe* [2003] equation, the plotting positions of the experimental data (shown in Figure 6 as symbols) are slightly different from those presented in *Wilcock and Crowe* [2003] because, for consistency, this analysis applied the resistance equations presented in this paper to calculate shear stress instead of applying the normal flow assumption used in the original analysis.

[31] It can be observed in Figure 6 that the $W_j^* \sim \tau/\tau_{ij}$ relation by *Parker* [1990] is steeper than that of *Wilcock and Crowe* [2003], and the W_j^* values calculated with *Parker* [1990] relation is generally higher than those calculated with *Wilcock and Crowe* [2003] relation for higher τ/τ_{ij} values. As a result, a trial TUGS model run is conducted by replacing the original *Wilcock and Crowe* [2003] $W_j^* \sim \tau/\tau_{ij}$ relation with that of *Parker* [1990]. To be consistent with *Wilcock and Crowe's* [2003] equation, dimensionless sediment transport rate for the *Parker* [1990] $W_j^* \sim \tau/\tau_{ij}$ relation is adjusted to 0.002 from its original value of 0.00218, which is a relatively minor adjustment:

Simulated results by replacing Equation (1) with Equation (22) are presented in Figures 7, 8, and 9, for Runs 1, 2, and 3, respectively. Comparison of profiles in Figures 7a, 8a, and 9a shows that numerical simulation adequately reproduced the observed bed profile as indicated by the very close bed slope between numerical simulation and observation,

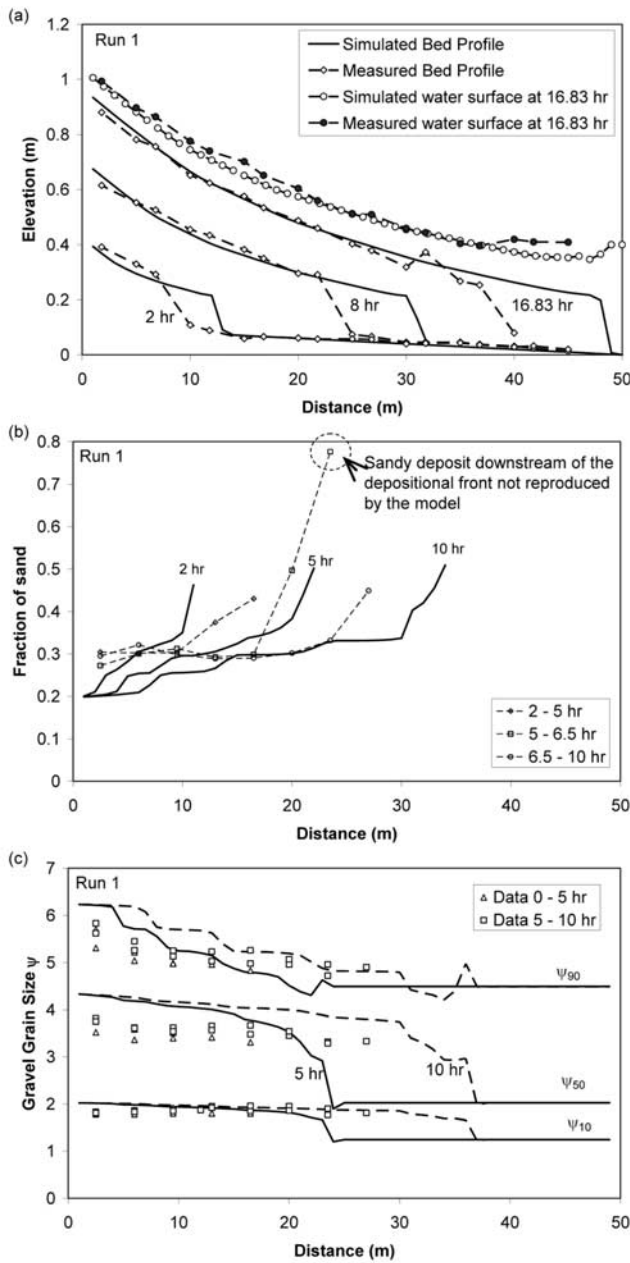


Figure 7. Simulated (a) bed profile, (b) sand fraction; and (c) characteristic gravel grain size in the deposit for Run 1 by replacing Wilcock and Crowe’s dimensionless sediment transport rate \sim normalized shear stress relation with that of Parker [1990]. In (c), the lines are predicted results, alternating between solid and dashed lines at different times for better visualization.

improving significantly from the original simulation results as presented in Figures 5a and 5b. The simulated volume of sediment upstream of the depositional front remains to be higher than the observed value for all the three runs, most likely due to the fact that some fine sediment bypassed the depositional front in the flume experiment as discussed earlier. The model is unable to bypass the small amount of fine sediment through the depositional front, which is likely

an area for future improvement. Comparison between Figures 9b and 5d indicates that the simulated sand fractions in the deposit are slightly worse than the original simulation. Despite this slightly decreased simulation quality, the simulated sand fraction adequately matches those observed in the experiments as shown in Figures 7b, 8b, and 9b. Comparisons between simulation and flume experiment in Figures 7c, 8c, and 9c indicate that the adjusted model

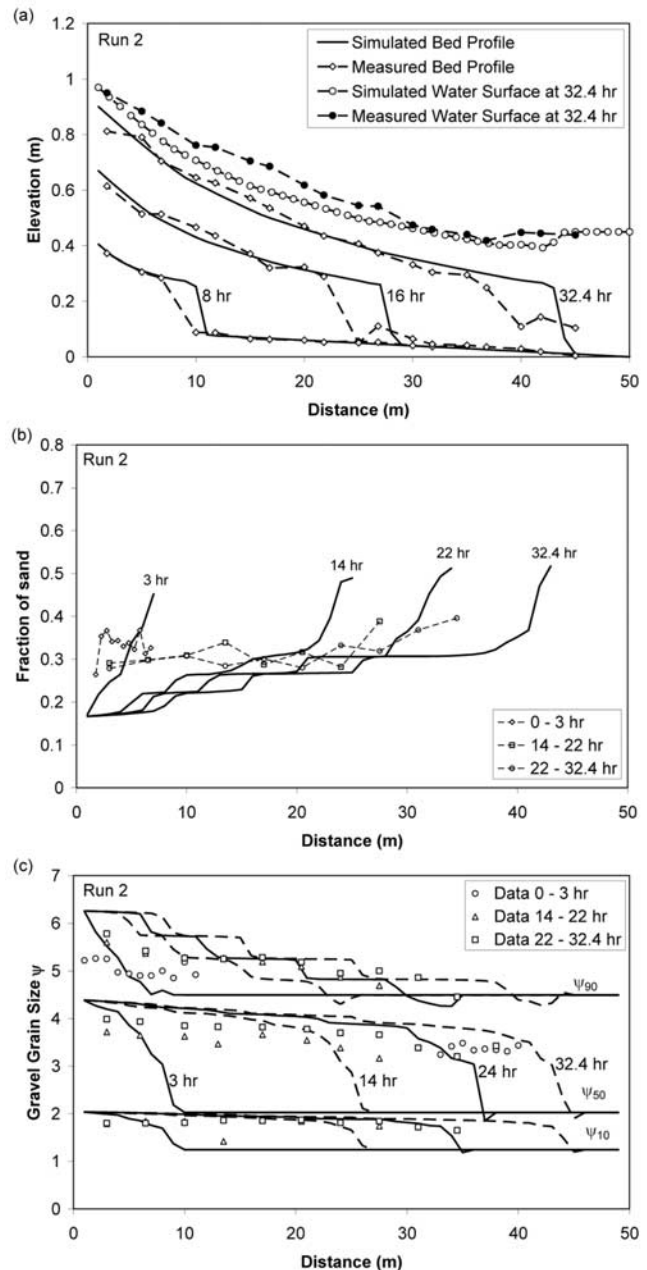


Figure 8. Simulated (a) bed profile, (b) sand fraction; and (c) characteristic gravel grain size in the deposit for Run 2 by replacing Wilcock and Crowe’s dimensionless sediment transport rate \sim normalized shear stress relation with that of Parker [1990]. In (c), the lines are predicted results, alternating between solid and dashed lines at different times for better visualization.

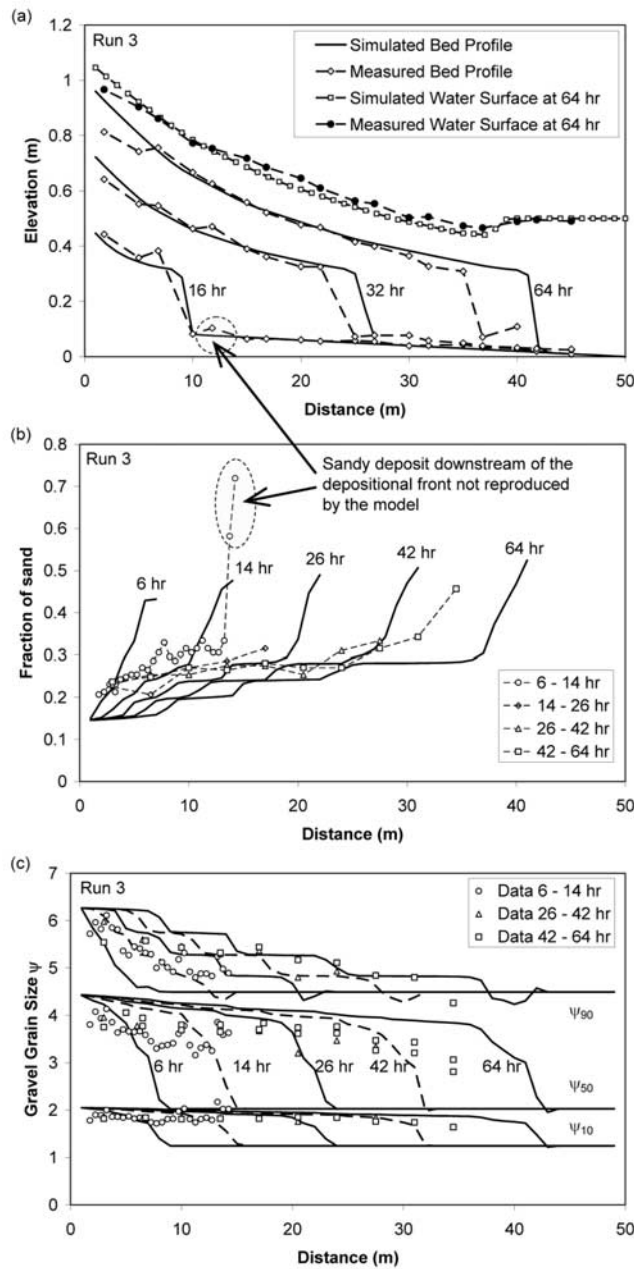


Figure 9. Simulated (a) bed profile, (b) sand fraction; and (c) characteristic gravel grain size in the deposit for Run 3 by replacing Wilcock and Crowe's dimensionless sediment transport rate \sim normalized shear stress relation with that of Parker [1990]. In (c), the lines are predicted results, alternating between solid and dashed lines at different times for better visualization.

adequately reproduced subsurface gravel characteristic grain sizes, similar to the original model.

9.3. Discussions on the SAFL Downstream Fining Simulation

[32] Comparison between simulated and observed sedimentation process for the three SAFL downstream fining runs indicated that TUGS model, with slight modification to

the equation of Wilcock and Crowe's [2003], adequately reproduced general bed slope, the subsurface gravel characteristic grain sizes, and the fraction of sand in the deposit. The area where the model needs improvement is that numerical simulation over predicted the volume of sediment deposition upstream of the depositional front due to the fact that the model was unable to bypass the small amount of fine sand through the depositional front to the impoundment area. In other word, the model under predicted the transport rate for the finest fraction of the sand class when shear stress is low (i.e., in the ponded area). Even without further improvement, the model should perform reasonably well in simulating sediment transport under most circumstances judged by the good agreement between the simulation and flume experiment in bed slope, gravel grain size, and sand fractions in the deposit. If we consider the under prediction of the finest fraction of the sand class under low shear stress as a systematic error in the predicted sediment transport rate, this error is no more than 10% of the overall sediment transport rate for the cases simulated, judged by the no more than 10% of over deposition of the sediment volume upstream of the depositional front. In all the practical problems, the relative error in sediment supply, which serves as model input, is usually much larger than 10%, making a 10% relative error in predicted transport rate acceptable. This argument can also be corroborated by the sediment transport \sim shear stress data such as shown in Figure 6, where both W_j^* and τ/τ_{ij} are plotted in log-scale, and for any given τ/τ_{ij} value, W_j^* varies by more than an order of magnitude.

10. Examination of Sand Entrainment With Flushing Flow Flume Experiment of Wu and Chou [2003]

[33] Wu and Chou [2003] conducted a flushing flow experiment with a 40-cm wide flume. The flume is 7.2-m long with a 2.5-m long section in the middle designated as the experimental section. The flume is set at a slope of 0.01, a typical value for gravel bedded rivers. A gravel mix with grain size ranging between 2 and 50.8 mm and a sand mix with grain size ranging between 0.5 and 2 mm are used for the experiment. In the experimental section, a mixture of 32% sand mix and 68% gravel mix was placed in the flume with a thickness of 10 cm. The reaches upstream and downstream of the experimental section were placed with 10-cm thick gravel mix without sand. In order to observe the effect of flushing flow, a constant discharge of 68 l/s was sent through the flume for 7 h. To sample fine sediment fractions in the deposit through time, the experimental section was divided into three reaches, each occupies a third of the 2.5-m experimental zone. The three reaches were named Reaches 1, 2, and 3 from upstream to downstream. Bed material was sampled by inserting capped 9-cm diameter 6-cm long cylinders into the deposit at different times during the run and leaving them until the end of the run. The cylinders had caps that prevent further fine sediment flushing and preserved the samples for grain size analysis at the end of the experiment. Upon finishing the experiment, the samples within the cylinders were divided into two 3-cm subsamples, with the upper sample termed as surface and bottom sample termed as subsurface. The surface and subsurface samples were analyzed separately

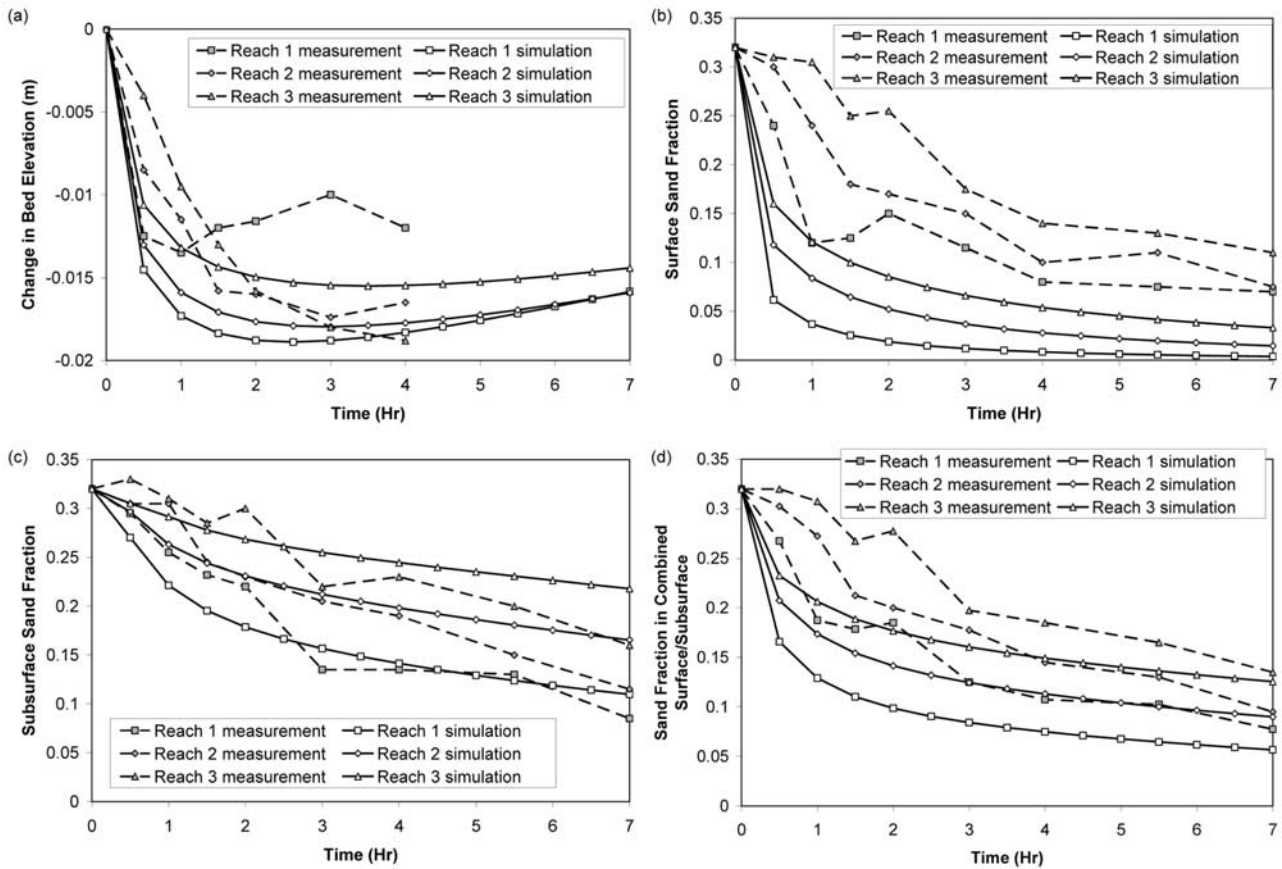


Figure 10. Comparison of simulated and observed results for the *Wu and Chou* [2003] flushing flow experiment: (a) changes in bed elevation; (b) surface layer sand fraction; (c) subsurface sand fraction; and (d) sand fraction in the combined surface and subsurface sample. The predicted results are solid lines and the measured results are symbols connected with dashed lines.

to obtain sand fraction values. During the experiment, 3 kg of gravel was added to the upstream end of the flume as a slug in every 30 min. More details of the experiment can be found in the original reference [Wu and Chou, 2003].

[34] Simulation of the *Wu and Chou* [2003] flushing flow experiment with TUGS model followed exactly the same procedure as the flume experiment described above. Similar to the simulation of the SAFL experiments, abrasion coefficient β_a was set to zero due to the limited channel length. Because there is no fine sediment infiltration within the experimental zone, coefficient a_i in Equation (11b) is set to 0. Similar to the simulation of SAFL downstream fining runs, initial porosity of the gravel and sand deposit is set at 0.3 and both the surface layer thickness and parameter H_{ci} in Equation (19) are set to 3 cm to be consistent with *Wu and Chou's* [2003] sampling protocol. Because there was no lateral sediment input during the experiment, both q_{gl} and q_{sl} are initially set to zero for the simulation. Note that while q_{gl} remains to be zero throughout the simulation, q_{sl} will become higher than zero during simulation because the entrained sediment during flushing flow is wrapped into this term with the application of Equation (20).

[35] Several trials are needed for adjusting coefficient a_c in Equation (11a) in order to achieve a reasonable fit between the flume experiment and numerical simulation. The results presented below used the unmodified *Wilcock and Crowe* [2003] equation and a coefficient a_c value of 0.02.

[36] Comparison of simulated and observed results is presented in Figure 10, which indicates that numerical simulation reasonably reproduced changes in bed elevation, subsurface sand fraction and sand fraction in combined surface/subsurface sample, while the simulated surface layer has less fine sediment than the sampling indicated. The original publication of *Wu and Chou* [2003] compared the change in bed elevation, surface sand fraction, and subsurface sand fraction. Here I added the comparison of sand fraction in the combined surface and subsurface sample. Because of the way the samples were separated into the surface and subsurface layers, the sand fractions in combined surface and subsurface samples should be more reliable than the data for surface and subsurface samples. The photograph showing channel bed before and after flushing flow by *Wu and Chou* [2003], for example, indicated that the post-flushing channel surface for Reach 2 is relatively free of sand, indicating that the way to separate the 6-cm samples into surface and subsurface sub-samples may have somewhat influenced the surface sand fraction data.

[37] Note that the formulation for sediment infiltration (Equation (11b)) is not tested in this paper. It is presented here as a compliment to the entrainment formulation because infiltration can be important in short-term and can act to negate the entrainment at long-term basis. Both Equations (11a) and (11b), although somewhat useful in providing fine sediment infiltration and entrainment information if cali-

brated to the specific river reach, should be replaced with more physically based equations that need minimal or no calibration, once such equations are available. For long-term simulations under natural conditions, it can be assumed that the entrainment and infiltration of sand achieve a dynamic balance, and thus, can be neglected in the simulation by setting both a_i and a_e to zero such as in the simulation of the SAFL downstream fining experiments. In a paper submitted concomitantly to River Research and Applications [Cui, 2007], I examine the dynamics of sand fractions in Sandy River, Oregon, including the sedimentation process upstream of Marmot Dam and a 50-km reach between Marmot Dam and Columbia River Confluence under the assumption that $a_i = 0$ and $a_e = 0$.

11. Conclusions

[38] The Unified Gravel-Sand (TUGS) model is developed based on *Wilcock and Crowe's* [2003] bed load equation, the gravel transfer function of *Hoey and Ferguson* [1994] and *Toro-Escobar et al.* [1996], a hypothetical sand transfer function during bed aggradation, and hypothetical subsurface sand entrainment/infiltration functions. The model, without adjustment to any coefficient in the *Wilcock and Crowe's* [2003] equation, are applied to simulate three relatively large-scale flume experiments and produced excellent agreements between simulated and measured characteristic gravel grain sizes and fraction of sand in the deposits. The unmodified model, however, over-predicted the bed slope for all the runs, and a minor adjustment to the model produced good agreements in bed profiles, gravel characteristic grain sizes and sand fractions in the deposits for all the three runs. To test the performance of sand entrainment from subsurface deposit, the model is tested against the flushing flow data of *Wu and Chou* [2003] with reasonable results. This reasonable agreement, nevertheless, should not be interpreted as an indication that the model can simulate sand entrainment accurately for other situations. What it suggests is that, the model can be used for simulation of fine sediment entrainment if adequate calibration is conducted. More physically based fine sediment entrainment and infiltration functions are needed so that the model can be applied in rivers with minimal or no calibration in simulating short-term events such as fine sediment entrainment during and fine sediment infiltration after the release of a flushing flow.

Notations

a_e, a_i coefficients in entrainment and infiltration functions;
 B channel width;
 D_j particle diameter separating the (j-1)-th and j-th size groups;
 \bar{D}_j mean particle diameter of the j-th size group, $\bar{D}_j = \sqrt{D_j D_{j+1}}$;
 D_{gs} geometric mean grain size of sand;
 D_{sg} surface geometric mean grain size for the combined sand and gravel;
 D_{sgg} surface geometric mean grain size of the gravel;
 F_j fraction of j-th size group of the surface layer gravel;
 F_j' aerial fraction of the j-th size group of surface layer gravel;
 F_r Froude number;

F_{rm} critical Froude number that defines whether to apply the backwater equation or the quasi-normal flow assumption;
 F_s surface layer sand fraction;
 F_{se} equilibrium surface sand fraction for sand entrainment;
 f_{ij} fraction of the j-th size group of the gravel class for sediment that transfers from the bed load and surface layer to the subsurface;
 f_{is} sand fraction of the sediment that transfers from the bed load and surface layer to the subsurface;
 f_s sand fraction within subsurface sediment deposit;
 f_{se} equilibrium subsurface sand fraction for sand infiltration;
 g acceleration of gravity;
 h water depth;
 k_s roughness height;
 L_a surface layer thickness;
 p_j fraction of the j-th size group of the gravel class in bed load;
 Q_g volumetric transport rate of gravel;
 Q_s volumetric transport rate of sand;
 Q_w water discharge;
 q_e upward sand flux per unit area from subsurface sand entrainment;
 q_{gl} lateral volumetric gravel supply rate per unit channel length;
 q_{glj} lateral volumetric gravel supply rate of the j-th size group per unit channel length;
 q_i downward sand flux per unit area from sand infiltration;
 q_{sl} lateral volumetric sand supply rate per unit channel length;
 q_{sv} net upward flux from combined sand entrainment and infiltration;
 S bed slope or water surface slope;
 S_0 local bed slope;
 S_f local friction slope;
 t time;
 v_s settling velocity of fine sediment particles;
 W_i^* dimensionless sediment transport rate;
 β_a volumetric abrasion coefficient of gravel;
 χ coefficient in gravel transfer function;
 η thickness of the sediment deposit;
 λ_p porosity of the sediment deposit;
 ρ density of water;
 σ_{gg} geometric standard deviation of subsurface gravel;
 σ_{sgg} geometric standard deviation of surface layer gravel;
 τ shear stress;
 τ_{ri} reference shear stress;
 τ_{rm} reference shear stress for surface geometric mean grain size;
 ψ_j grain size psi-scale associated with grain size D_j , $\psi_j = \log_2(D_j)$.

[39] **Acknowledgments.** Funding for model development is provided by CALFED Ecosystem Restoration Program (Grant ERP-02D-P61) and The Nature Conservancy (TNC). I thank Keith Barnard, Matt Brown, Geoff Hales, Graham Matthews, Scott McBain, Jess Newton and John Wooster for providing bulk sampling data, Rebecca Soileau for providing her experimental data, and Peter Wilcock for making his experimental data available on the Web. The assistance, comments and critiques from Christian Braudrick, Bill Dietrich, Mike Fainter, Mike Roberts, Jeremy Venditti and John Wooster are gratefully acknowledged. I would also like to

thank Stillwater Sciences for providing financial support during the draft and revisions of this manuscript. The useful comments from Rob Ferguson, Marwan Hassan, two anonymous reviewers, associate editors (André Roy and Tammo Steenhuis) and the editor (Scott Tyler) have been incorporated into the manuscript.

References

- Beacham, T. D., and C. B. Murray (1990), Temperature, Egg Size, and Development of Embryos and Alevins of Five Species of Pacific Salmon: A Comparative Analysis, *Transactions of the American Fisheries Society*, vol. 119, 927–945.
- Beschta, R. L., and W. L. Jackson (1979), The intrusion of fine sediments into a stable gravel bed, *J. Fish. Res. Board Ca.*, 36, 204–210.
- CDWR (California Dept. of Water Resources) (1994), San Joaquin River tributaries spawning gravel assessment, Stanislaus, Tuolumne, and Merced Rivers, Appendix C: Bulk sampling data, surface and subsurface, September.
- CDWR (California Dept. of Water Resources) (1995), Sacramento River gravel study – Keswick Dam to Cottonwood Creek, *Memorandum to Stacy Cepello, Environmental Specialist IV, and Koll Buer, Senior Engineering Geologist*, October 20.
- Coble, D. W. (1961), Influence of water exchange and dissolved oxygen in redds on survival of steelhead trout embryos, *Trans. Am. Fish. Soc.*, 90, 469–474.
- Cooper, A. C. (1965), The effects of transported stream sediments on the survival of sockeye and pink salmon eggs and alevin, *Bulletin 18, International Pacific Salmon Fisheries Commission*, New Westminster, British Columbia, Canada.
- Cui, Y. (2007), Examining the dynamics of grain size distributions of gravel/sand deposits in the Sandy River, Oregon with a numerical model, *River Research and Applications*, 23, 732–751, doi:10.1002/tra.1012.
- Cui, Y., and G. Parker (1997), A quasi-normal simulation of aggradation and downstream fining with shock fitting, *Int. J. Sediment Res.*, 12(2), 68–82.
- Cui, Y., and G. Parker (1998), The arrested gravel-front: stable gravel-sand transitions in rivers. Part 2: General numerical solution, *J. Hydraul. Res.*, 36(2), 159–182.
- Cui, Y., and G. Parker (2005), Numerical model of sediment pulses and sediment supply disturbances in mountain rivers, *J. Hydraul. Eng.*, 131(8), 646–656, doi:10.1061/(ASCE)0733-9429(2005)131:8(646).
- Cui, Y., and A. C. Wilcox (2007), Numerical modeling of sediment transport upon dam removal: application to Marmot Dam in Sandy River, Oregon, Chapter 23 in *Sedimentation Engineering, ASCE Manual 110*, M. H. Garcia, in press.
- Cui, Y., G. Parker, and C. Paola (1996), Numerical simulation of aggradation and downstream fining, *J. Hydraul. Res.*, 32(2), 185–204.
- Cui, Y., G. Parker, T. E. Lisle, J. Gott, M. E. Hansler-Ball, J. E. Pizzuto, N. E. Allmendinger, and J. M. Reed (2003a), Sediment pulses in mountain rivers, Part I: Experiment, *Water Resour. Res.*, 39(9), 1239, doi:10.1029/2002WR001803.
- Cui, Y., G. Parker, J. E. Pizzuto, and T. E. Lisle (2003b), Sediment pulses in mountain rivers, Part II: Comparison between experiments and numerical predictions, *Water Resour. Res.*, 39(9), 1240, doi:10.1029/2002WR001805.
- Cui, Y., G. Parker, T. E. Lisle, J. E. Pizzuto, and A. M. Dodd (2005), More on the evolution of bed material waves in alluvial rivers, *Earth Surf. Proc. Landforms*, 30, 107–114, doi:10.1002/esp.1156.
- Cui, Y., C. Braudrick, W. E. Dietrich, B. Cluer, and G. Parker (2006a), Dam Removal Express Assessment Models (DREAM), Part 2: Sensitivity tests/sample runs, *J. Hydraul. Res.*, 44(3), 308–323.
- Cui, Y., G. Parker, C. Braudrick, W. E. Dietrich, and B. Cluer (2006b), Dam Removal Express Assessment Models (DREAM), Part 1: Model development and validation, *J. Hydraul. Res.*, 44(3), 291–307.
- Diplas, P., and G. Parker (1985), Pollution of gravel spawning grounds due to fine sediment, *Project Report No. 240*, St. Anthony Falls Laboratory, Univ. of Minnesota, Minneapolis, Minnesota, 131 pp.
- Ferguson, R. I. (2003), Emergence of abrupt gravel-to-sand transitions along rivers through sorting processes, *Geology*, 31(2), 159–162, doi:10.1130/0091-7613(2003)031<0159:EOAGTS>2.0.CO;2.
- Graham Matthews and Associates (2001), Gravel quality monitoring in the mainstem Trinity River, Final Report prepared for Trinity County Board of Supervisors, January, 21 p + figures and appendices.
- Graham Matthews and Associates (2003a), WY2003 geomorphic monitoring report, Report to Western Shasta Resource Conservation District, Anderson, CA.
- Graham Matthews and Associates (2003b), Hydrology, geomorphology, and historic channel changes of Lower Cottonwood Creek, Shasta and Tehama Counties, California, Report to National Fish and Wildlife Foundation, CALFED Bay Delta Program Project # 97-N07.
- Graham Matthews and Associates (2004), WY2004 geomorphic monitoring report, Report to Western Shasta Resource Conservation District, Anderson, CA.
- Han, Q. W., Y. C. Wang, and X. L. Xiang (1981), Initial dry density of sediment deposit, *J. Sediment Research*, Issue 1, (in Chinese).
- Hirano, M. (1971), River bed degradation with armoring, *Proc. Jpn. Soc. Civil Eng.*, 195, 55–65.
- Hirsch, C. (1989), Numerical Computation of Internal and External Flows, Volume 1: Fundamentals of Numerical Discretization, John Wiley & Sons, New Ed Edition, 538 p, ISBN-10:04719238501.
- Hoey, T. B., and R. I. Ferguson (1994), Numerical simulation of downstream fining by selective transport in gravel bed rivers: Model development and illustration, *Water Resour. Res.*, 30, 2251–2260.
- Komura, S. (1963), Discussion of “sediment transport mechanics: Introduction and properties of sediment,” *J. Hydraul. Division, ASCE*, 89(1), 263–266.
- Paola, C., G. Parker, R. Seal, S. K. Sinha, J. B. Southard, and P. R. Wilcock (1992), Downstream fining by selective deposition in a laboratory flume, *Science*, 258, 1757–1760.
- Parker, G. (1990), Surface-based bedload transport relation for gravel rivers, *J. Hydraul. Res.*, 28(4), 417–436.
- Parker, G. (1991a), Selective sorting and abrasion of river gravel, I: Theory, *J. Hydraul. Eng.*, 117(2), 131–149.
- Parker, G. (1991b), Selective sorting and abrasion of river gravel, II: Application, *J. Hydraul. Eng.*, 117(2), 150–171.
- Parker, G., and A. J. Sutherland (1990), Fluvial armor, *J. Hydraul. Res.*, 28(5), 529–544.
- Phillips, R. W., R. L. Lantz, E. W. Claire, and J. R. Moring (1975), Some effects of gravel mixtures on emergence of coho salmon and steelhead trout fry, *Trans. Am. Fish. Soc.*, 104, 461–466.
- Ribberink, J. (1987), Mathematical modeling of one-dimensional morphological changes in rivers with non-uniform sediment, Ph.D. Thesis, Delft Univ. of Technology, the Netherlands.
- Seal, R., C. Paola, G. Parker, and B. Mullenbach (1995), Laboratory experiments on downstream fining of gravel, narrow channel runs 1 through 3: supplemental methods and data, *External Memorandum M-239*, St. Anthony Falls Laboratory, Univ. of Minnesota.
- Seal, R., C. Paola, G. Parker, J. B. Southard, and P. R. Wilcock (1997), Experiments on downstream fining of gravel: 1. Narrow-channel runs, *J. Hydraul. Eng.*, 123(10), 874–884, doi:10.1061/(ASCE)0733-9429(1997)123:10(874).
- Stillwater Sciences (2002), Dam Removal Express Assessment Models (DREAM), *Technical Report*, 62p, October 2002, available at <http://www.stillwatersci.com/publications/DREAM.pdf>, accessed in June 2006.
- Toro-Escobar, C. M., G. Parker, and C. Paola (1996), Transfer function for the deposition of poorly sorted gravel in response to streambed aggradation, *J. Hydraul. Res.*, 34(1), 35–54.
- Wilcock, P. R. (1998), Two-fraction model of initial sediment motion in gravel-bed rivers, *Science*, 280, 410–412.
- Wilcock, P. R., and J. C. Crowe (2003), Surface-based transport model for mixed-size sediment, *J. Hydraul. Eng.*, 129(2), 120–128.
- Wilcock, P. R., and S. T. Kenworthy (2002), A two-fraction model for the transport of sand/gravel mixtures, *Water Resour. Res.*, 38(10), 1194, doi:10.1029/2001WR000648.
- Wilcock, P. R., G. M. Kondolf, W. V. G. Matthews, and A. F. Barta (1996), Specification of sediment maintenance flows for a large gravel-bed river, *Water Resour. Res.*, 32, 2911–2921.
- Wu, F. C., and Y. J. Chou (2003), Simulation of gravel-sand bed response to flushing flows using a two-fraction entrainment approach: Model development and flume experiment, *Water Resour. Res.*, 39(8), 1211, doi:10.1029/2003WR002184.
- Wu, W., and S. S. Y. Wang (2006), Formulas for sediment porosity and settling velocity, *J. Hydraul. Eng.*, doi:10.1061/(ASCE)0733-9429(2006)132:8(858), 858–862.

Y. Cui, Stillwater Sciences, 2855 Telegraph Avenue, Suite 400, Berkeley, CA 94705, USA. (yantao@stillwatersci.com)